INTERNATIONAL JOURNAL OF ENERGY STUDIES

e-ISSN: 2717-7513 (ONLINE); homepage: https://dergipark.org.tr/en/pub/ijes

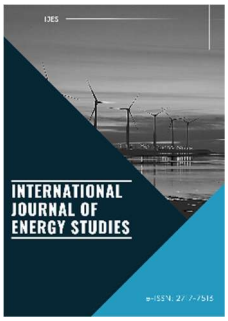

Research Article
Int J Energy Studies 2024; 9(3): 463-491
DOI: 10.58559/ijes.1491603

Received : 28 May 2024
Revised : 04 July 2024
Accepted : 08 July 2024

Exploring the future hydropower production of a run-of-river type plant in the source region of the Tigris Basin (Türkiye) under CMIP6 scenarios

Emrah Yalcin*
*Kırşehir Ahi Evran University, Department of Civil Engineering, Kırşehir, Türkiye, ORCID: 0000-0002-3742-8866
(*Corresponding Author: emrah.yalcin@ahievran.edu.tr)*

Highlights

- Climate projections indicate increasing temperature and decreasing precipitation trends.
- A warming climate is expected to alter the streamflow regime significantly.
- Less snowfall is projected in future winters compared to the past.
- Projected changes in hydro-climatic conditions could result in decreases of up to 17.3% in energy production.
- Adaptive measures are needed to achieve target returns from hydropower projects in the coming decades.

You can cite this article as: Yalcin E. Exploring the future hydropower production of a run-of-river type plant in the source region of the Tigris River (Türkiye) under CMIP6 climate change scenarios. Int J Energy Studies 2024; 9(3): 463-491.

ABSTRACT

This assessment presents a framework for exploring the changing climate impacts on the energy production capacity of a run-of-river type plant, using the Basoren Weir and Hydropower Plant (HPP) as a case study. The Basoren Project is planned considering historical streamflow records in the source region of the Euphrates-Tigris River Basin (ETRB), which is a prominent hotspot warming at nearly double the global average rate. The quantification is built on precipitation and maximum/minimum temperature datasets from 24 Global Climate Models (GCMs) belonging to the sixth phase of the Coupled Model Intercomparison Project (CMIP6) under the moderate- and high-end Shared Socioeconomic Pathway (SSP) scenarios of SSP2-4.5 and SSP5-8.5, as well as the CMIP6 historical experiment (HEXP) scenario. The distribution mapping method is employed to adjust the raw GCM datasets for systematic biases. The Soil and Water Assessment Tool (SWAT) is preferred in producing daily runoff time series for the bias-adjusted simulations of each GCM over the historical (1988-2009) and three future (2025-2049, 2050-2074, and 2075-2099) periods. The ramifications of the changing climate on the Basoren HPP's energy production capacity are assessed based on the medians of the operational results reached for each GCM under the future societal development scenarios of SSP2-4.5 and SSP5-8.5, considering the medians achieved under the HEXP scenario as the reference case. The results indicate potential reductions in the mean yearly energy production of the Basoren HPP by 7.9%, 5.5%, and 5.3% under the SSP2-4.5 scenario, and by 5.8%, 8.0%, and 17.3% under the SSP5-8.5 scenario for the periods 2025-2049, 2050-2074, and 2075-2099, respectively. While declining spillway releases are expected to partly offset the impact of decreasing streamflow rates on energy production, the shift from a snow-dominated to a rain-dominated hydrologic regime necessitates re-optimizing the power capacities of the ETRB plants to maintain effective use of hydropower potential.

Keywords: Climate change, CMIP6, SWAT, Hydropower, Türkiye

1. INTRODUCTION

Water resources are becoming increasingly susceptible to the consequences of climate variability and change on a global scale [1-5]. The ramifications of changing climate on water resources extend across multiple sectors, affecting energy, ecosystems, and human societies [6,7]. Renewable energy sources, such as hydropower and thermoelectric power, are particularly dependent on climate and are likely to be influenced by projected hydroclimatic changes [8-16]. As a key clean and renewable energy source, hydropower significantly contributes to climate change mitigation, accounting for over 16% of total electricity generation and about 85% of renewable electricity production globally [17]. Neglecting the impacts of changing climate on hydropower could result in suboptimal performance and economic inefficiencies in hydropower plant (HPP) projects [18-21]. The projected impacts of a changing climate on hydropower generation are not uniform and vary based on the specific location, size, and configuration of each project [22]. For instance, hydropower potential could decrease by up to 5.4% in China [23] and increase by up to 25% in India [24]. Therefore, a comprehensive understanding of current and future hydroclimatic conditions and their interactions with energy systems is crucial for informing sustainable hydropower generation at spatial and temporal scales pertinent to decision-making [25,26].

Such understanding requires the application of climate models, including Global Climate Models (GCMs) and Regional Climate Models (RCMs), to evaluate changing climate impacts on hydrological attributes and, consequently, energy production for HPP projects. The latest release of the Coupled Model Intercomparison Project, phase 6 (CMIP6), offers enhanced data from climate models based on socioeconomic scenarios named Shared Socioeconomic Pathways (SSPs) [27]. These SSPs are integral to a new scenario framework that aids researchers in understanding future climate impacts, vulnerabilities, adaptation strategies, and mitigation efforts [28]. The SSPs outline various potential future trajectories for land use changes and greenhouse gas emissions, derived from integrated assessment models with diverse assumptions regarding economic development, climate action measures, and international governance [29]. The judicious selection of appropriate GCMs or RCMs is pivotal for comprehending future impacts and effectively managing the opportunities and challenges posed by climate change, often achieved by using ensembles to mitigate uncertainty [30,31]. Although RCMs offer higher resolutions and incorporate intricate physical processes that enable them to replicate fine-scale climatic

information beyond the capabilities of GCMs [32], CMIP6-based RCMs are still relatively sparse compared to the tens of GCMs included in the CMIP6 database.

The Euphrates and Tigris are the two largest rivers of the Middle East region, identified as a prominent hotspot warming at nearly double the global average rate [33-36]. Originating in Türkiye, these rivers play a vital role in supporting hydropower production, irrigation, and domestic water supply for Türkiye, Syria, Iraq, and Iran. Bozkurt and Sen [37] reported that the snow-dominated northern highlands of the Euphrates-Tigris River Basin (ETRB) in Türkiye will experience the most significant direct impacts of changing climate compared to the other riparians. Projections from Bozkurt et al. [38], Sen et al. [39], and Yucel et al. [40] show that snowmelt runoff in the northern highlands of the watershed will occur earlier in the year. Despite these expected changes for the basin's streamflow regime, as documented also by several studies [41-48], Türkiye continues to expand its hydropower generation capacity on the ETRB by constructing new dam and run-of-river type plant projects, which are planned without accounting for the changing climate impacts. While the existing HPP projects with reservoirs offer the potential to mitigate climate change impacts by re-optimizing operational rule curves and adjusting reservoir operation levels accordingly, this adaptation opportunity does not exist for run-of-river type projects in operation. Therefore, it is imperative to consider changing climate conditions in the planning stages of run-of-river type plants.

The primary objective of this assessment is to explore the future energy production of a run-of-river type HPP in the most threatened highlands region of the ETRB under GCM projections from the CMIP6 database. The Basoren Weir and HPP Project, planned on one of the snow-fed upstream tributaries of the Tigris River, serves as the case study (Figure 1). For this purpose, daily precipitation and maximum/minimum temperature datasets from 24 CMIP6 GCMs under the CMIP6 historical experiment (HEXP) scenario and the moderate-end SSP2-4.5 and high-end SSP5-8.5 societal development scenarios [27] are utilized to project daily inflow rates and, subsequently, daily energy productions for the Basoren HPP in the historical period of 1988-2009 and three future periods: 2025-2049, 2050-2074, and 2075-2099. The Soil and Water Assessment Tool (SWAT) is selected for projecting daily streamflow rates at the Basoren Weir location under the bias-adjusted climate datasets of each GCM. A daily operational algorithm is developed relying on the technical features of the project specified in its feasibility report [49]. Operational runs are performed over the historical and future periods using the inflow projections obtained with the

calibrated SWAT model. The quantification of changing climate impacts is performed over the 2025-2049, 2050-2074, and 2075-2099 periods, on a seasonal and annual basis, considering the ensemble medians of the energy productions calculated for the climate simulations of each GCM under the scenarios of SSP2-4.5 and SSP5-8.5. The historical medians determined for the 1988-2009 period under the historical HEXP scenario serve as the reference case. This assessment aims to highlight the urgent necessity for developing adaptation and mitigation strategies in the planning of run-of-river type hydropower projects in the ETRB and other similar basins threatened by changing climate. Moreover, the analyses conducted on the ensemble medians of the hydro-climatological projections emphasize the importance of incorporating climate change impacts on spillway discharges and non-power releases for water supply, particularly for such snow-fed watersheds.

2. OVERVIEW OF THE BASOREN PROJECT

Bitlis Creek stands as a prominent tributary of the Tigris River ensconced within the territorial confines of Türkiye, alongside Botan, Batman, and Garzan Creeks. The Basoren Weir and HPP Project [49] is planned to be constructed on Bitlis Creek, approximately 13 km south of the Baykan district within the borders of Siirt province, as presented in Figure 1. The Basoren Project is an energy-constrained facility aimed at harnessing the hydropower potential of Bitlis Creek between elevations of 561 m and 530 m. The flows of Bitlis Creek, originating from a drainage area of 840.8 km^2, are planned to be diverted by a weir structure designed at the thalweg elevation of 553 m into a 5920 m-long trapezoidal transmission canal with a bed slope of 0.0004 m/m. This transmission also includes a 190 m-long concrete siphon structure with an inner diameter of 4.6 m. Subsequently, the flows will be conveyed to the power plant, equipped with four Francis turbines, by passing through a penstock 125 m in length and 4 m in diameter. The plant is designed to operate with an optimized discharge rate of 40 m^3/s, divided among four units with capacities of 2.50, 6.25, 15.625, and 15.625 m^3/s, culminating in a cumulative installed power capacity of 9.9 MW [49].

Karinca (E26A016) and Baykan (E26A010) are the two stream gauging stations (SGSs) measuring the runoffs of Bitlis Creek, as depicted in Figure 1. The drainage areas of the Karinca and Baykan SGSs are 346.4 and 636.5 km^2, respectively. While the Karinca SGS has only streamflow measurements for the 1965-1969 period, the Baykan SGS has daily flow measurements spanning from 1955 to 2010 [50]. As for *in-situ* climate data, Bitlis (17207) and Siirt (17210) are the two

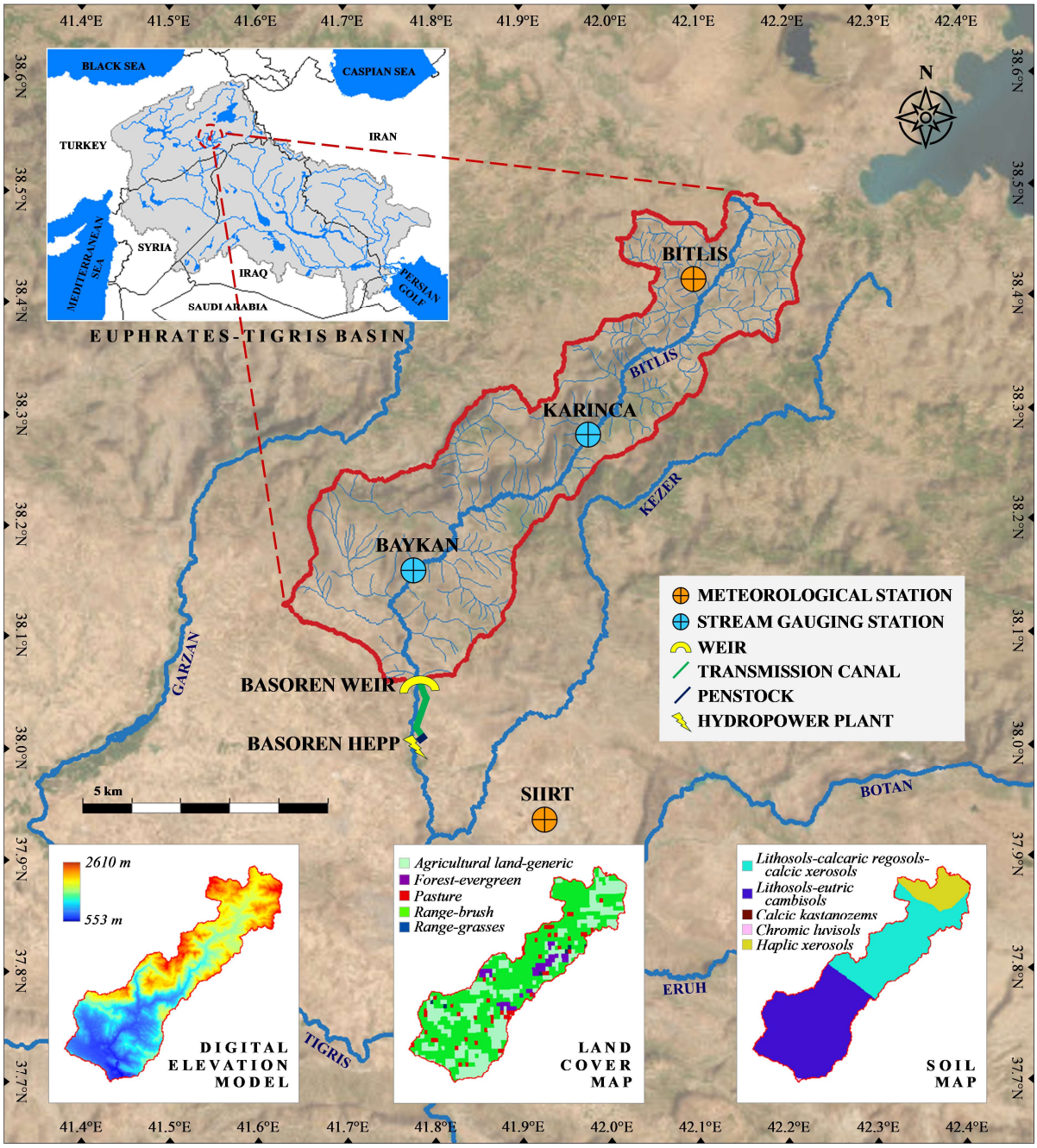

Figure 1. Layout map of the Basoren Weir basin along with geospatial characteristics

weather stations (WSs) around the Basoren Weir basin, with long-term continuous daily records of precipitation, maximum/minimum temperature, relative humidity, wind speed, and solar radiation (Figure 1) [51]. These weather datasets are essential for setting up the hydrologic model of the study basin. The Bitlis and Siirt WSs operate at altitudes of 1573 m and 895 m, respectively. According to the established Thiessen polygons, these stations represent 66.5% and 33.5%, respectively, of the Basoren Weir basin, which has an average elevation of 1442 m. Although the hydrological modeling timeline for the study could be extended from 1955 to 2010 considering

the available streamflow, precipitation, and temperature measurements from the synoptic stations, data availability for the other essential weather records limits the historical analysis period to 1988-2009 [50,52].

3. METHODOLOGY

3.1. Hydrological Modeling Using SWAT

The hydrological model of the Basoren Weir catchment is built using SWAT [53,54]. ArcSWAT 2012 (revision 664) is used to construct the SWAT model for simulating the daily inflow rates of the Basoren Weir under both historical and potential future climate scenarios. In configuring the model, the digital elevation model at 1 arc-second resolution [55], land cover map in grid format at 1 km spatial resolution [56], and grid-based soil characteristics map at a scale of 1:5 million [57] are utilized to delineate the basin's physiographic conditions, as presented in Figure 1. Daily measurements of precipitation, maximum/minimum temperature, relative humidity, wind speed, and solar radiation from the Bitlis and Siirt WSs for the 1984-2009 period are incorporated into the model [52]. This includes the weather records for a four-year warm-up period from 1984 to 1987 and the long-term mean monthly statistics of these measurements [51]. The integrated weather generator of SWAT utilizes these statistics to produce daily values, addressing any missing observations and generating both historical and future rates of relative humidity, wind speed, and solar radiation under the historical HEXP scenario and the future scenarios of SSP2-4.5 and SSP5-8.5. Additionally, five elevation bands are set up to consider the influence of the mountainous terrain on both precipitation and temperature in the simulation of snowpack and snowmelt processes [53,58].

After configuring the SWAT model, it undergoes calibration and validation for daily runoff simulations against the measured runoff data from the Baykan SGS [50] spanning 1988 to 2009. The periods from 1988-2001 and 2002-2009 are designated for calibration and verification, respectively. For the sensitivity analysis of modeling parameters, as well as the calibration and verification stages, the Sequential Uncertainty Fitting Version 2 (SUFI-2) algorithm [59,60] is preferred within the SWAT Calibration and Uncertainty Procedures (SWAT-CUP) software [58]. The objective function used is the $b\mathrm{R}^2$ statistic, which is the product of the coefficient of determination (R^2) and the slope of the zero-intercept linear regression line between the measured and simulated data (b). SUFI-2 allocates uncertainties from the input datasets, conceptual model, and modeling parameters across the sensitive parameters' ranges iteratively. Simulation

uncertainty is measured using the 95% prediction uncertainty (95PPU) band. This band is evaluated using the *P*-factor and *R*-factor indices. The *P*-factor represents the percentage of the measured data that falls within the band, whereas the *R*-factor signifies the ratio of the mean band width to the standard deviation of the measured data. Typically, a greater *P*-factor requires a correspondingly larger *R*-factor. Thus, SUFI-2 is iterated multiple times, progressively narrowing the initial parameter ranges until an optimal set is reached. The calibrated parameter ranges are provided by the last iteration, and the best simulation with the highest objective function value from this iteration yields the best-performing parameter values [61].

In this study, a three-step sequential calibration procedure is applied for the developed SWAT model to mitigate snow-related parameter dependency and identifiability challenges. In the initial two steps of the calibration procedure, the precipitation and temperature lapse rates and snow-related sensitive parameters are calibrated and then set to their best simulation values sequentially. In the subsequent third step, the procedure is finalized by calibrating the ranges of other streamflow-related sensitive parameters. At the start of each calibration step, the sensitivity of each parameter is examined independently by undertaking a *one-at-a-time* analysis, employing a single iteration that consists of 50 simulations. Subsequently, a combined iteration comprising 500 simulations is carried out with the sensitive modeling parameters of that step, assigning their initial ranges determined through the *one-at-a-time* analyses. The combined iterations persist until satisfactory levels of *P*-factor, *R*-factor, and bR^2 are achieved. The final iteration in the third step of the calibration procedure provides the calibrated parameter ranges and best-performing parameter values [59,62].

Following the completion of model calibration, the calibrated parameter ranges undergo validation against the daily flow records from 2002 to 2009. This validation entails a single combined iteration using the calibrated parameter ranges. Beyond the bR^2 metric, the ratio of the root means square error to the standard deviation of the measured data (RSR), Nash-Sutcliffe Efficiency (NSE) [63], and percent bias (PBIAS) indices are utilized to evaluate the calibration and validation performances for the best simulation results. However, it's crucial to note that these statistical measures derived from the best simulation outputs do not fully capture the flow forecasting ability of the calibrated model due to the dependency of the best simulation on the highest objective function value attained against the historical streamflow measurements. Therefore, a single simulation is repeated for the validation period to affirm the efficacy of the best-performing

parameter set identified for the calibration period. The results of this simulation are denoted as the best simulation estimates [62], and the flow forecasting efficacy of the calibrated model is scrutinized based on this simulation's outputs, employing the bR^2, NSE, PBIAS, and RSR metrics.

3.2. CMIP6 GCM Datasets and Daily Streamflow Projections

The daily precipitation and maximum/minimum temperature simulations of the 24 CMIP6 GCMs at the Bitlis and Siirt WSs' coordinates are used to drive the calibrated SWAT model for projecting the daily inflow rates of the Basoren Weir under the historical HEXP scenario and the moderate- and high-end societal development scenarios of SSP2-4.5 and SSP5-8.5. Details of the GCMs selected due to their daily time-scale simulations under the first ensemble member (r1i1p1f1) for the analyzed SSP scenarios are given in Table 1. The raw GCM datasets are obtained from the website of the Earth System Grid Federation (ESGF) [64]. Since the downloaded GCM datasets have different grid sizes, they are transformed to a standardized spatial resolution of 0.5° x 0.5° using the first-order conservative remapping technique [65] to facilitate consistency and comparability.

The raw historical and future simulations extracted from the transformed GCM datasets undergo bias adjustment against the synoptic stations' measurements [52] to align them with location-specific climate features, including distribution, sequence, and magnitude. The bias adjustments are conducted using the distribution mapping (DM) method of the Climate Model Data for Hydrologic Modeling (CMhyd) software [66]. The modified index of agreement (*md*) [67], normalized root means square error (nRMSE) [68], Kling-Gupta efficiency metric (KGE) [69], and fraction skill score (FSS) [70] statistics are utilized as the performance metrics to assess the effectiveness of the performed bias adjustment over the historical datasets of the GCMs.

The inflow rates of the Basoren Weir under the historical HEXP scenario over the 1988-2009 period are estimated with the calibrated SWAT model by introducing the bias-adjusted precipitation and maximum/minimum temperature simulations from each GCM for the period from 1984 to 2009. This process involves conducting 24 model runs, utilizing the initial four years' datasets to warm up the model. To project the inflow rates of the Basoren Weir over the period 2025-2099, a total of 48 model runs are conducted utilizing the bias-adjusted simulations of each GCM for the 2021-2099 period under the SSP2-4.5 and SSP5-8.5 scenarios. To ensure fair comparisons between the streamflow projections and, hence, hydropower productions over the

historical and future periods, all model runs are executed under representative daily relative humidity, wind speed, and solar radiation rates generated by SWAT.

Table 1. Overview of the GCMs selected from the CMIP6 database

Model ID	Country	Spatial resolution in arc degrees	
		Latitude	Longitude
ACCESS-CM2	Australia	1.25	1.875
ACCESS-ESM1-5	Australia	1.25	1.875
BCC-CSM2-MR	China	1.112-1.121	1.125
CanESM5	Canada	2.767-2.791	2.8125
CMCC-ESM2	Italy	0.9424084	1.25
EC-Earth3	Europe	0.696-0.702	0.703125
EC-Earth3-CC	Europe	0.696-0.702	0.703125
EC-Earth3-Veg	Europe	0.696-0.702	0.703125
EC-Earth3-Veg-LR	Europe	1.112-1.121	1.125
FGOALS-g3	China	2.025-5.181	2
GFDL-CM4	USA	1	1.25
GFDL-ESM4	USA	1	1.25
INM-CM4-8	Russia	1.5	2
INM-CM5-0	Russia	1.5	2
IPSL-CM6A-LR	France	1.267606	2.5
KIOST-ESM	Korea	~1.9	1.875
MIROC6	Japan	1.389-1.401	1.40625
MPI-ESM1-2-HR	Germany	0.927-0.935	0.9375
MPI-ESM1-2-LR	Germany	1.850-1.865	1.875
MRI-ESM2-0	Japan	1.112-1.121	1.125
NESM3	China	1.850-1.865	1.875
NorESM2-LM	Norway	1.894737	2.5
NorESM2-MM	Norway	0.9424084	1.25
TaiESM1	Taiwan	0.9424084	1.25

3.3. Hydropower Production under Changing Climate

The consequences of the changing climate on the hydropower production capacity of the Basoren HPP are analyzed using an operational algorithm coded in the Visual Basic for Applications (VBA) language. The operational runs are conducted on a daily time scale, relying on the technical characteristics and operational constraints of the project [49]. The applied operational algorithm is schematically illustrated in Figure 2. The technical features integrated into the operational algorithm include the weir crest elevation, tailwater level, spillway capacity, design discharge, number of units, type of turbines, turbine capacities, and turbine efficiency curve (i.e., load-versus-efficiency), as well as the transmission canal, siphon structure, and penstock characteristics.

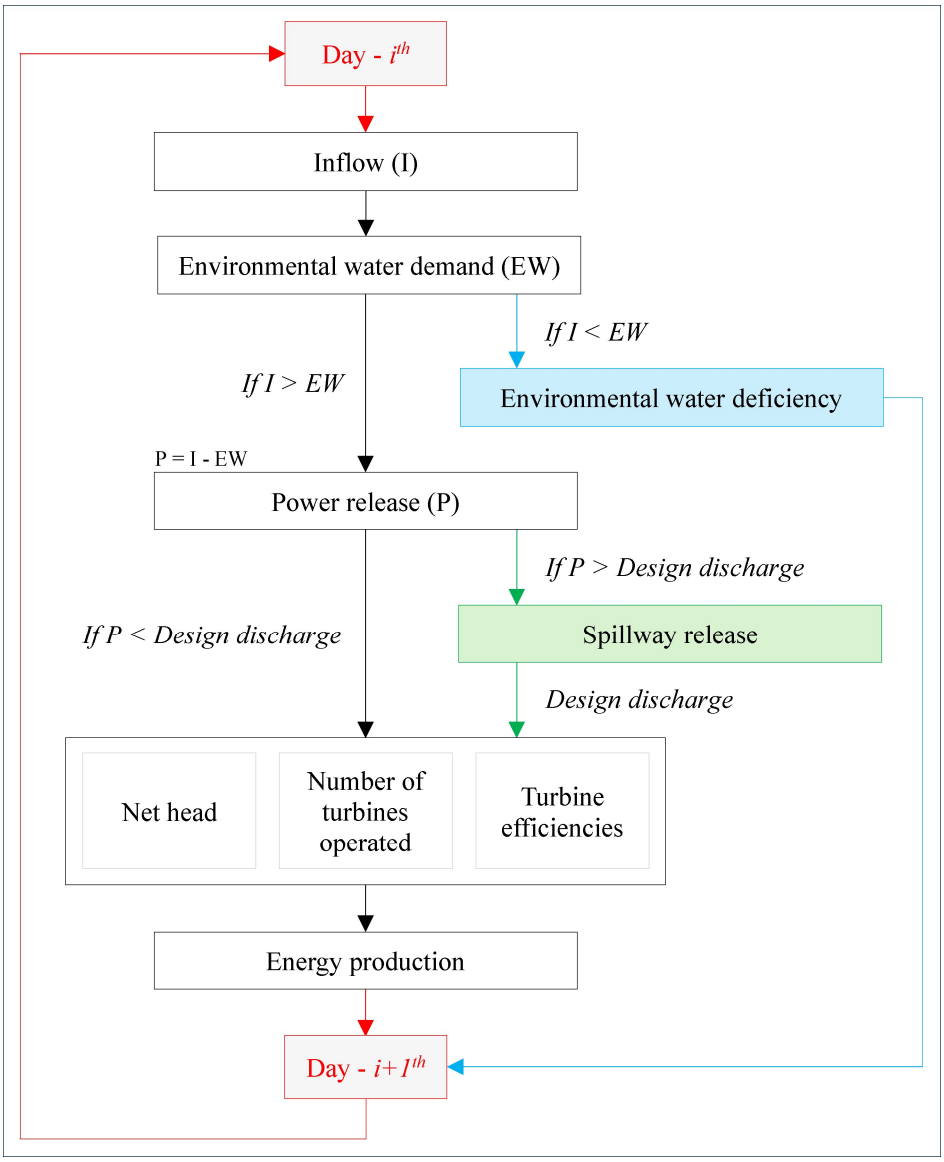

Figure 2. Schematic representation of the operational algorithm of the Basoren Project

Additionally, due to the transmission canal involved in the project design, a total of 69.98 hm^3 of water in varying amounts monthly is mandated to be released annually as environmental water (i.e., non-power release) for the creek section between the weir and the outlet of the power station to sustain the natural ecosystem.

In addition to these fixed inputs, the streamflow projections obtained for the Basoren Weir location are utilized as dynamic inputs for repeated operations. Accordingly, a total of 24 operations are executed in the 1988-2009 period using the streamflow projections attained from the bias-adjusted climate simulations of the considered GCMs under the historical HEXP scenario. The potential future variations in the hydropower production of the Basoren HPP are investigated over the

periods of 2025-2049, 2050-2074, and 2075-2099. For each future time frame evaluated, the operational runs are repeated 48 times utilizing the streamflow time series estimated for the bias-corrected climate simulations of the GCMs in the scenarios of SSP2-4.5 and SSP5-8.5. The variations in hydropower production, as well as spillway and environmental water releases, are assessed over three future time frames, considering the operational results attained for the period 1988-2009 as the reference scenario.

4. RESULTS AND DISCUSSIONS

4.1. Evaluation of the Calibrated SWAT Model Performance

The calibration of the SWAT model is performed through a three-step procedure for the period 1988-2001, using the daily runoff measurements from the Baykan SGS. Initially, two lapse rate parameters and six snow-related sensitive modeling parameters are calibrated and set to their best-performing values in the first and second steps, respectively. In the subsequent third step, the parameter ranges of 12 sensitive streamflow-related modeling parameters are refined through repeated combined iterations until a satisfactory simulation performance is achieved. Detailed information about the calibrated parameters is presented in Table 2. In this table, the operator *v* denotes the replacement of a parameter value within the defined range, whereas the operator *r* denotes a relative adjustment obtained by multiplying the current parameter value by 1 plus a value within the specified range. Additionally, fixed values mean that a parameter is initially adjusted at that step and then maintained constant in the subsequent steps.

The 95PPU band and the best simulation time series attained over the final combined iteration are presented in Figure 3(a). The resulting 95PPU band has a *P*-factor statistic of 0.89 and an *R*-factor statistic of 0.95. A *P*-factor statistic surpassing 0.7 and an *R*-factor statistic below 1.5 are deemed sufficient to strike a balance between the two metrics for runoff simulations [61]. The bR^2, NSE, PBIAS, and RSR statistics of the best simulation against the station records are computed, in turn, as 0.76, 0.68, 4.6%, and 0.56 (Table 3). Daily runoff simulations of catchment-scale models are classified as *satisfactory* if they achieve an R^2 statistic exceeding 0.6 with a *b* value around 1, an NSE statistic surpassing 0.5, and a PBIAS statistic within the range of ±15% [71]. Furthermore, a runoff simulation is considered *satisfactory* if it achieves an RSR value below 0.7 [72]. According to the attained statistics and graphical time series, it can be concluded that the best simulation performance of the calibrated model is sufficient to be categorized as *satisfactory*.

Table 2. List of the sensitive modeling parameters along with calibrated ranges and best-performing values

Step	Parameter [53,54]	Operator	Calibrated range	Best-performing value
1	TLAPS.sub	*v*	-	-7.05
	PLAPS.sub	*v*	-	9.26
2	SMFMX.bsn	*v*	-	3.31
	SFTMP.bsn	*v*	-	1.62
	SMTMP.bsn	*v*	-	-2.47
	SNOCOVMX.bsn	*v*	-	38.86
	SMFMN.bsn	*v*	-	1.39
	TIMP.bsn	*v*	-	0.75
3	ALPHA_BF.gw	*v*	[0, 1]	0.77
	OV_N.hru	*r*	[-0.9, 199]	156.82
	RCHRG_DP.gw	*v*	[0, 1]	0.59
	CH_K2.rte	*v*	[-0.01, 500]	462.5
	SOL_BD().sol	*r*	[-0.3, 0.66]	0.06
	SOL_K().sol	*r*	[-0.99, 249.31]	15.28
	CN2.mgt	*r*	[-0.1, 0.1]	-0.07
	GWQMN.gw	*v*	[0, 5000]	4455
	GW_REVAP.gw	*v*	[0.02, 0.2]	0.16
	GW_DELAY.gw	*v*	[0, 500]	400.5
	SOL_AWC().sol	*r*	[-0.99, 4.71]	-0.51
	SOL_Z().sol	*r*	[-0.7, 2.33]	0.95

Figure 3(b) displays the daily runoff rates simulated by the model for the Baykan SGS location during the validation period from 2002 to 2009. Similar to the calibration phase, the verification phase results in a reasonable 95PPU band characterized by adequate observed data coverage and narrowness, with values of 0.87 and 1.10 for the *P*-factor and *R*-factor metrics, respectively [61]. Furthermore, the performance of the best simulation closely resembles that of the calibration period, achieving *satisfactory* bR^2, NSE, PBIAS, and RSR values of 0.74, 0.64, 10.2%, and 0.60, respectively (Table 3) [71,72]. When assessing the forecasting ability of the developed model using the best-performing parameter set from the calibration, the best simulation estimates exhibit

Table 3. Simulation statistics for the performance evaluation of the SWAT model

Simulation	R^2	*b*	NSE	PBIAS (%)	RSR	Mean (m^3/s)		Standard deviation (m^3/s)	
						Simulated	Observed	Simulated	Observed
Calibration period (1988-2001)									
Best simulation	0.76	1.00	0.68	4.6	0.56	17.18	18.02	29.18	25.54
Validation period (2002-2009)									
Best simulation	0.74	1.01	0.64	10.2	0.60	16.08	17.90	26.58	22.70
Best simulation estimates	0.74	0.99	0.65	6.6	0.59	16.71		26.14	

performance comparable to that of the best simulation of the verification, as illustrated in Figure 3(b). As detailed in Table 3, the bR^2, NSE, PBIAS, and RSR metrics for the best simulation estimates are determined to be 0.73, 0.65, 6.6%, and 0.59, respectively.

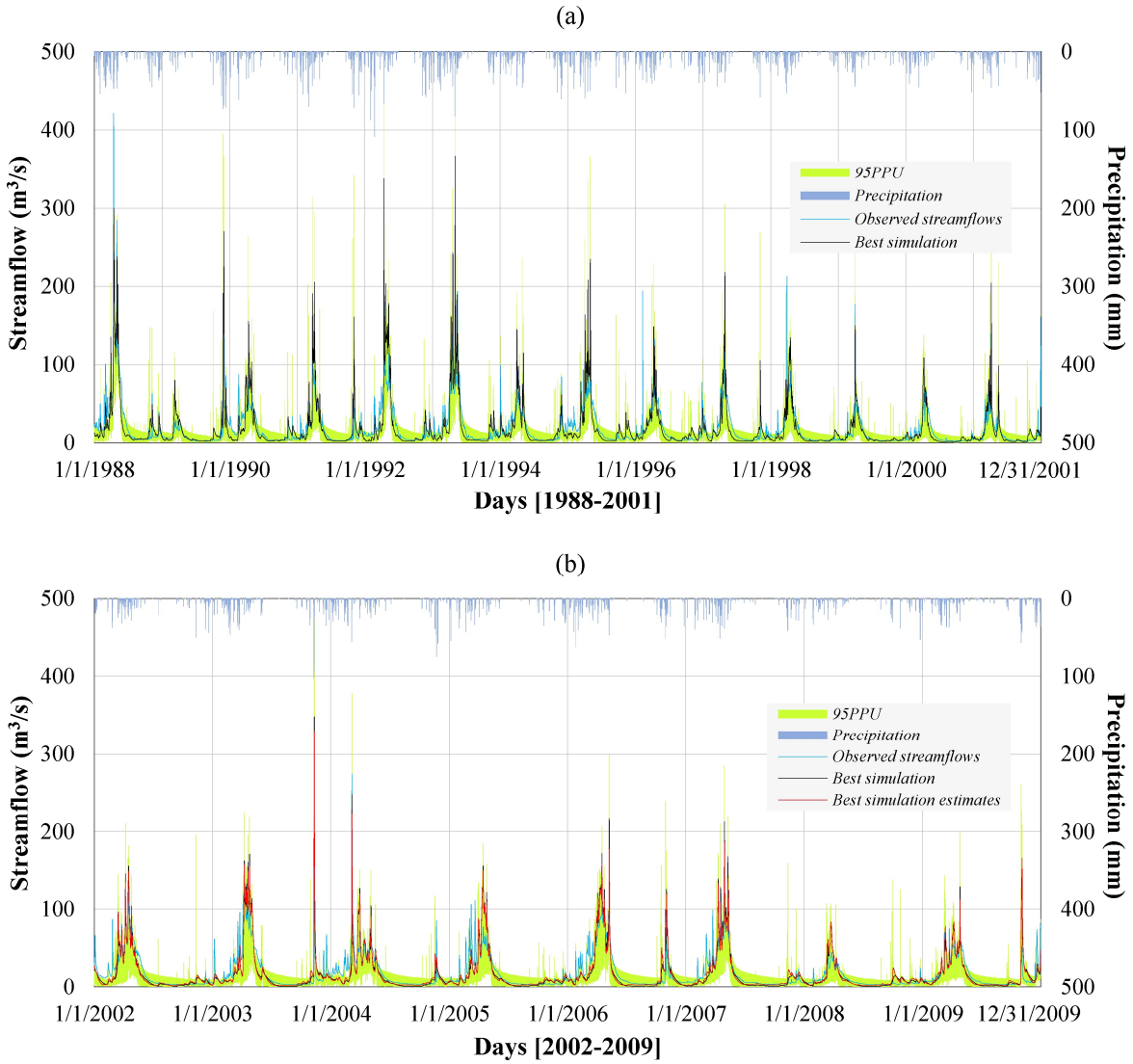

Figure 3. Comparison of the measured and simulated daily runoff rates at the Baykan SGS location over the **(a)** calibration and **(b)** validation periods

4.2. Projected Changes in Climate

Ensuring reliable streamflow projections hinges on effectively adjusting biases in GCM simulations. This study employs the DM method for the bias correction of the historical and future climate simulations from the 24 GCMs and four error indices to evaluate the simulation performances of the raw and bias-adjusted historical datasets against the records of the synoptic stations. While perfect agreement is indicated by 0 for the nRMSE metric, this value is 1 for the

md, KGE, and FSS statistics. Figure 4 illustrates the box-and-whisker plots of the areal-averaged performance metrics computed against the measurements of the Bitlis and Siirt stations on a monthly basis considering the stations' representation ratios for the Basoren Weir basin (i.e., 66.5% for the Bitlis WS and 33.5% for the Siirt WS). While significant error variabilities are observed for the raw climate datasets of the HEXP scenario, the error ranges diminish notably after bias

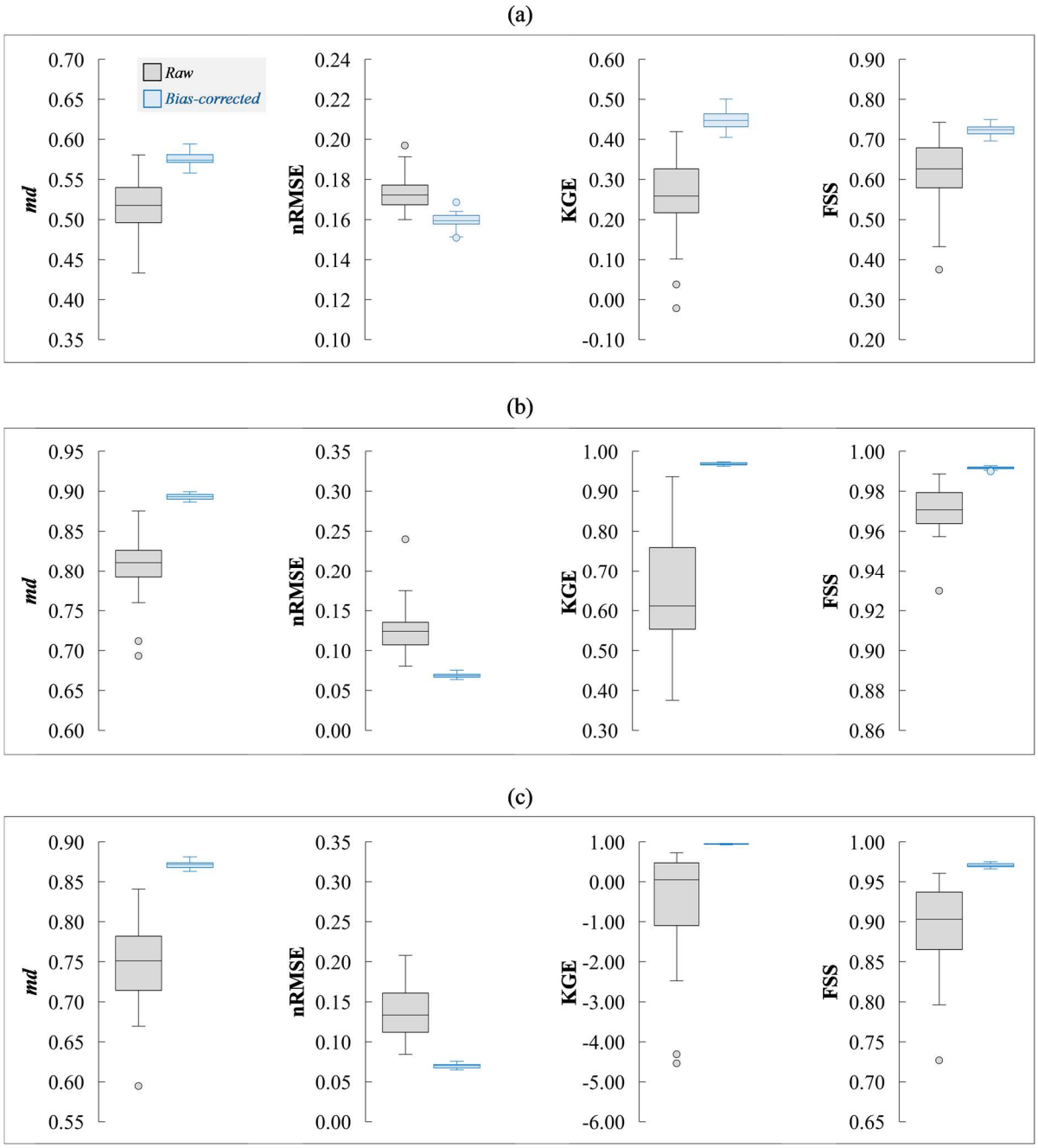

Figure 4. Comparison of performance statistics for the raw and bias-adjusted **(a)** precipitation, **(b)** maximum temperature, and **(c)** minimum temperature simulations of the GCMs across the Basoren Weir basin

correction. Specifically, the applied bias correction leads to nearly perfect alignments for the temperature datasets of the GCMs. Although the statistical improvement for the precipitation simulations lags behind that for the temperature simulations, this is a common problem also mentioned by other authors using different bias adjustment methods [47,48,73-75]. Nevertheless, while the areal-averaged mean yearly precipitation and maximum/minimum temperature rates for the Basoren Weir basin based on the stations' records in the 1988-2009 period are 2.85 mm/day and 17.96°C/6.85°C, respectively, the corresponding median rates for the bias-adjusted GCM simulations under the historical HEXP scenario are determined as 2.75 mm/day and 18.07°C/6.97°C.

The areal-averaged annual mean precipitation and temperature time series of the 24 GCMs under the historical HEXP scenario and the future development scenarios of SSP2-4.5 and SSP5-8.5 for the Basoren Weir basin are illustrated in Figures 5(a-c), as their ensemble medians and 95% confidence intervals. Potential future climatic changes in the Basoren basin are assessed on a mean seasonal and annual basis for the median rates of the areal-averaged climate simulations of the GCMs under the scenarios of SSP2-4.5 and SSP5-8.5, utilizing the ensemble medians from the historical HEXP scenario as the reference case. As detailed in Table 4, this analysis is performed over the 2025-2049, 2050-2074, and 2075-2099 periods. Accordingly, for the SSP2-4.5 scenario, while the projected average annual and seasonal daily precipitation amounts show no substantial changes over the entire future period, the projected mean annual maximum/minimum temperature rates exhibit gradual increases, reaching 3.38°C/3.17°C in the period 2075-2099. For the SSP5-8.5 scenario, the average annual daily precipitation rate decreases by 6.7%, 8.5%, and 16.2% in the 2025-2049, 2050-2074, and 2075-2099 periods, respectively. The highest seasonal precipitation reductions are detected for the 2075-2099 period, with rates of 17.9%, 12.5%, 19.1%, and 24.2% for the autumn, winter, spring, and summer months, respectively. In this high-end SSP scenario, the average annual maximum/minimum temperatures during the periods of 2025-2049, 2050-2074, and 2075-2099 are anticipated to exceed those of the reference period by 2.10°C/1.91°C, 3.90°C/3.66°C, and 6.17°C/5.67°C, respectively. The foreseen precipitation and temperature anomalies for the Basoren Weir basin are highly consistent with the climate projections for the neighboring upstream tributaries of the Tigris River, attained under the moderate- and high-end SSP scenarios using different bias correction and ensembling techniques [47,48].

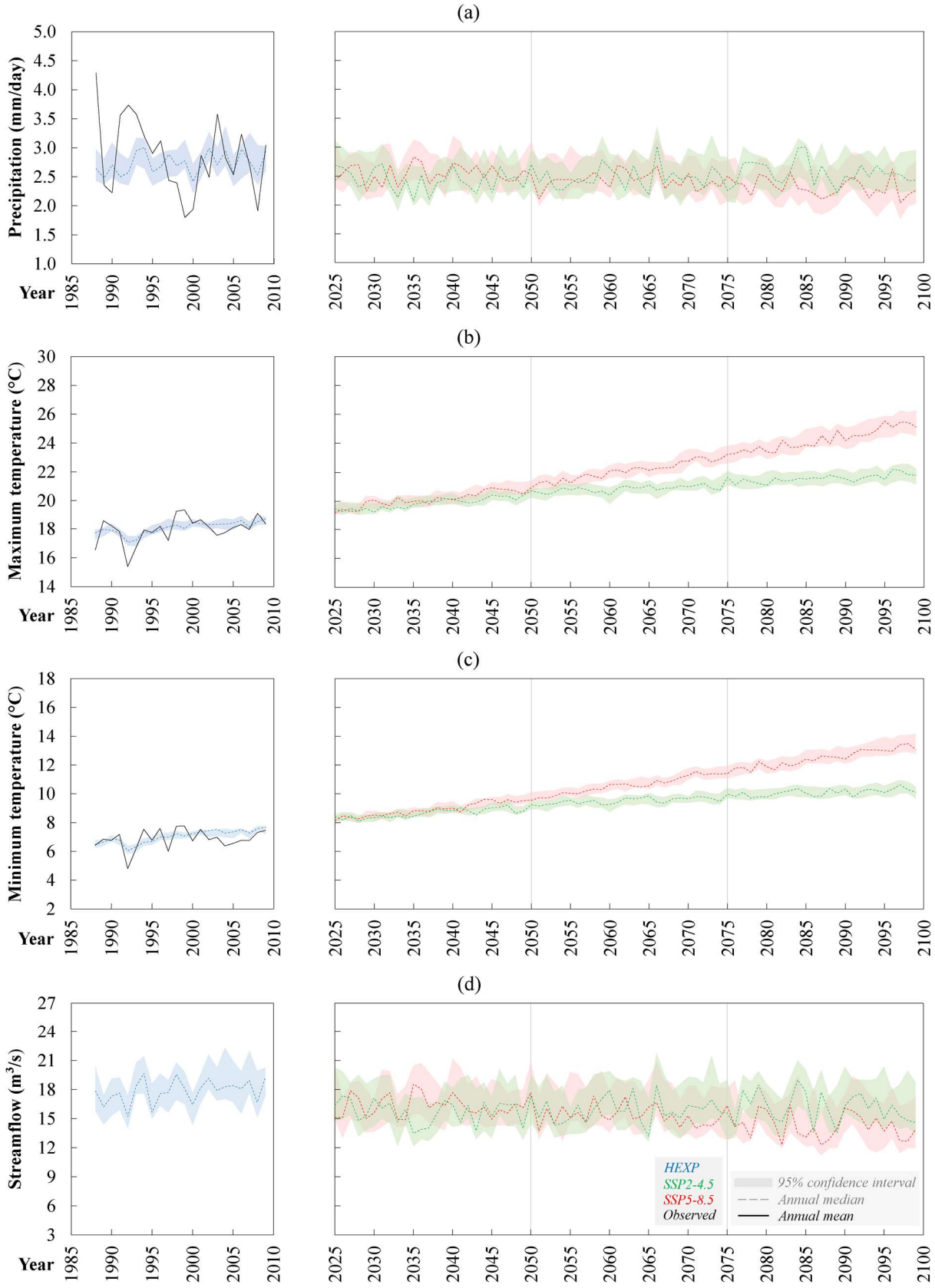

Figure 5. Annual **(a)** precipitation, **(b)** maximum temperature, and **(c)** minimum temperature projections for the Basoren Weir basin, along with **(d)** annual streamflow estimates at the Basoren Weir location

4.3. Projected Changes in Streamflow Regime

The historical and future daily inflow rates of the Basoren Weir are projected within the SWAT model utilizing the best-performing parameter values from the calibration. These projections rely on the bias-adjusted daily precipitation and maximum/minimum temperature datasets from the 24 GCMs under the historical HEXP scenario and the moderate- and high-end societal development scenarios of SSP2-4.5 and SSP5-8.5. The annual means of the resulting 24 daily streamflow time series for each climate scenario are depicted in Figure 5(d) as their ensemble medians and 95% confidence intervals. As with the analysis of climatic change, the median inflow rates obtained under the historical HEXP scenario serve as the reference case. Potential future variations in the inflow rates of the Basoren Weir are assessed based on the ensemble medians achieved under the scenarios of SSP2-4.5 and SSP5-8.5. As outlined in Table 4, this assessment is conducted on a mean seasonal and annual basis for the 2025-2049, 2050-2074, and 2075-2099 periods.

Table 4. Comparisons of the median precipitation and maximum/minimum temperature projections for the Basoren Weir basin and of the median inflow projections for the Basoren Weir

Climate scenario		HEXP	SSP2-4.5			SSP5-8.5		
Analysis period		1988-2009	2025-2049	2050-2074	2075-2099	2025-2049	2050-2074	2075-2099
Precipitation (mm/day)	Autumn	2.27	2.05	2.15	2.07	2.07	2.03	1.86
	Winter	4.59	4.28	4.36	4.45	4.46	4.35	4.01
	Spring	3.92	3.72	3.65	3.88	3.51	3.47	3.17
	Summer	0.26	0.25	0.23	0.25	0.25	0.25	0.19
	Annual	*2.75*	*2.57*	*2.59*	*2.66*	*2.57*	*2.51*	*2.30*
Maximum temperature (°C)	Autumn	20.66	22.57	23.59	24.26	23.11	24.88	27.44
	Winter	4.53	6.37	7.39	8.10	6.65	8.45	10.81
	Spring	15.40	16.91	17.62	18.32	17.14	19.00	21.04
	Summer	31.46	33.17	34.18	34.89	33.53	35.30	37.43
	Annual	*18.07*	*19.81*	*20.75*	*21.45*	*20.17*	*21.96*	*24.24*
Minimum temperature (°C)	Autumn	8.50	10.03	10.85	11.44	10.51	12.14	14.05
	Winter	-3.08	-1.45	-0.79	0.05	-1.28	0.17	1.60
	Spring	5.20	6.44	7.21	7.72	6.54	7.94	9.66
	Summer	17.10	19.34	20.64	21.18	19.59	22.08	25.04
	Annual	*6.97*	*8.63*	*9.52*	*10.14*	*8.88*	*10.63*	*12.64*
Streamflow rate (m^3/s)	Autumn	5.68	5.23	5.59	5.90	6.10	5.36	5.03
	Winter	15.17	15.90	18.27	19.39	16.57	19.54	21.06
	Spring	43.77	36.06	34.84	34.46	36.19	32.58	24.25
	Summer	7.69	6.62	6.47	6.65	6.76	6.37	5.68
	Annual	*18.13*	*15.98*	*16.31*	*16.62*	*16.43*	*15.97*	*13.99*

For the SSP2-4.5 scenario, the mean yearly inflow rate of the Basoren Weir decreases by 11.8%, 10.0%, and 8.3% in the periods 2025-2049, 2050-2074, and 2075-2099, respectively. In this moderate-end SSP scenario, the most outstanding streamflow variations are detected for the winter and spring seasons. While the average inflow rate for the spring months decreases by 17.6%, 20.4%, and 21.3% in the 2025-2049, 2050-2074, and 2075-2099 periods, respectively, increases of 4.8%, 20.4%, and 27.8% are anticipated for the winter rates of the corresponding periods. For the SSP5-8.5 scenario, the decrease percentages in the mean annual inflow rate are determined to be 9.4%, 11.9%, and 22.8% for the 2025-2049, 2050-2074, and 2075-2099 periods, respectively. In this high-end SSP scenario, the declines in the spring flow rates and the increases in the winter flows are foreseen to be much stronger than those in the SSP2-4.5 scenario. The mean winter inflows in the 2025-2049, 2050-2074, and 2075-2099 periods are anticipated to be 9.2%, 28.8%, and 38.8% higher than the historical mean inflow rate, respectively. In comparison, the decline percentages for the corresponding spring seasons are attained, in turn, to be 17.3%, 25.6%, and 44.6%. Such a shift projected for the future streamflow regime at the Basoren Weir location is also mentioned in other studies performed on streamflow projections for the neighboring upstream tributaries of the Tigris River [47,48]. Hence, given the climate projections for the Basoren basin under the scenarios of SSP2-4.5 and SSP5-8.5, it is reasonable to infer that precipitation in future winters will occur less frequently as snow compared to the past, due to the increasing temperature trends across the region. This inference aligns with the projections of Şensoy et al. [46] regarding the future snow duration, snow cover extent, and snow water equivalent in the snow-dominated headwater sub-catchments of the Euphrates River Basin, which share similar climatic and topographical characteristics with the Basoren basin.

4.4. Projected Changes in Hydropower Production

The annual means of the resulting energy production, power release, spillway release, and non-power (i.e., environmental water) release time series from the operation studies, conducted across the historical and future periods utilizing the daily inflow projections, are demonstrated in Figures 6(a-d), as their ensemble medians and 95% confidence intervals. Similar to the analyses for future climate and streamflow variations, the medians of the energy production and release amounts for the 24 different streamflow time series projected for the historical HEXP scenario serve as the reference case for the analysis of potential operational changes in the Basoren HPP. The median results of the operational studies for the period 1988-2009 reveal that the Basoren HPP has an average annual energy production of 26.29 GWh. Additionally, the mean yearly volume of water

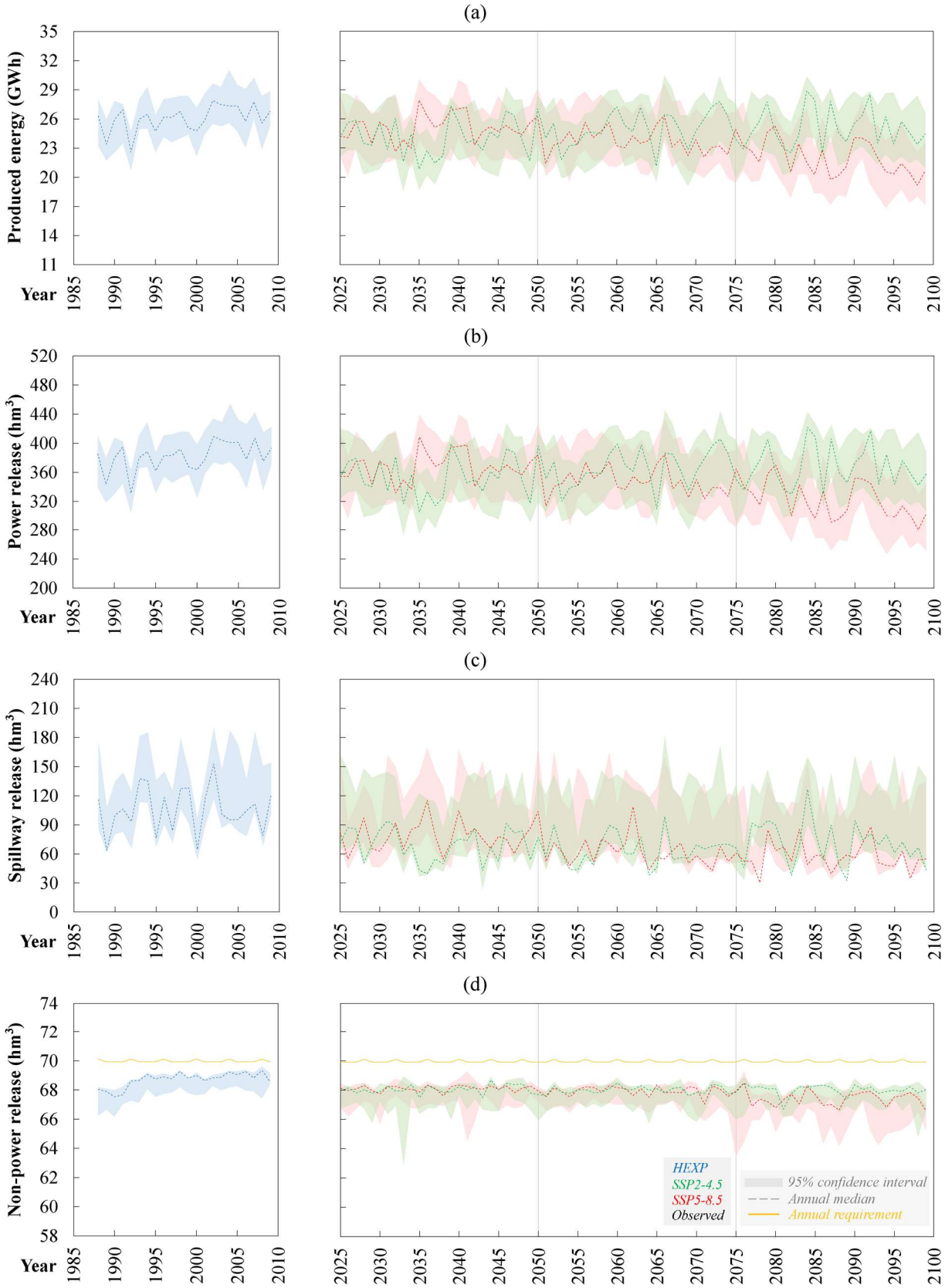

Figure 6. Annual **(a)** energy production, **(b)** power release, **(c)** spillway release, and **(d)** non-power release projections for the Basoren Project

passing through the turbines is projected to be 385.55 hm^3. It is noted that an average of 116.79 hm^3 of water is discharged annually from the spillway, with an additional 68.42 hm^3 released per year into the streambed to maintain ecosystem continuity. The spillway operates, on average, for 36 days per year, with 32 of those days occurring in spring. Moreover, an average annual deficiency of 2.2% in meeting environmental water demand is detected, rising to 22.5% during autumn.

As detailed in Table 5, the ensemble median operational results observed for the scenarios of SSP2-4.5 and SSP5-8.5 over the 2025-2049, 2050-2074, and 2075-2099 periods are compared to those achieved for the historical scenario on a mean seasonal and annual basis. For the SSP2-4.5 scenario, it is anticipated that the mean annual runoff rates at the Basoren Weir location will decrease by 11.8%, 10.0%, and 8.3% during the periods 2025-2049, 2050-2074, and 2075-2099, respectively (Table 4). The conducted operations indicate that the impact of the foreseen inflow decreases on future energy production is partly compensated by substantial declines in spillway releases. The mean yearly energy production of the Basoren HPP is determined, in turn, to be 7.9%, 5.5%, and 5.3% less than the historical average for the corresponding periods. Additionally, the mean annual amounts of water discharged through the spillway in these periods decline by 25.6%, 24.4%, and 24.0%, respectively. While the mean annual amount of spillway release for the spring seasons of the historical analysis period is 104.70 hm^3, this amount decreases to 69.12, 65.44, and 63.05 hm^3 for the periods of 2025-2049, 2050-2074, and 2075-2099, respectively. Furthermore, during these periods, it is observed that 33.5%, 35.8%, and 35.8% of the environmental water demand for the autumn months could not be met, respectively. For the SSP5-8.5 scenario, the decrease rates for the mean annual energy productions over the 2025-2049, 2050-2074, and 2075-2099 periods are determined as 5.8%, 8.0%, and 17.3%, respectively. In comparison, the mean yearly streamflow rates for the corresponding time frames decrease, in turn, by 9.4%, 11.9%, and 22.8% (Table 4). Similar to the projections under the SSP2-4.5 scenario, significant decreases of 24.0%, 33.3%, and 43.8% are observed in the mean annual spilled water amounts for these periods, respectively. The gradual reduction in the spring spillway releases reaches up to 69.2% in the 2075-2099 period. For the spring months of this period, the spillway is projected to operate for only 8 days per year on average. Moreover, the environmental water deficiency for the autumn months is expected to increase by 34.1%, 36.5%, and 42.2% in these future periods, respectively. Regardless of the SSP scenario considered, it is evident that the

anticipated financial gains from the Basoren Project, designed based on historical streamflow records [49], could not be realized in the face of shifting climate conditions over the basin.

Table 5. Comparisons of the median operation projections for the Basoren Project

Climate scenario		HEXP	SSP2-4.5			SSP5-8.5		
Analysis period		1988-2009	2025-2049	2050-2074	2075-2099	2025-2049	2050-2074	2075-2099
Produced energy (GWh/year)	Autumn	2.20	2.08	2.00	1.96	2.06	1.97	1.79
	Winter	6.88	7.15	8.07	8.48	7.34	8.43	9.12
	Spring	13.51	11.87	11.75	11.33	12.18	10.88	8.25
	Summer	3.70	3.14	3.02	3.12	3.19	2.92	2.59
	Annual	*26.29*	*24.23*	*24.84*	*24.89*	*24.77*	*24.19*	*21.75*
Power release (hm^3/year)	Autumn	32.53	30.50	29.34	28.77	30.35	28.86	26.41
	Winter	100.93	104.79	118.01	123.87	107.42	123.17	132.99
	Spring	197.16	173.12	171.30	165.31	177.72	158.66	120.48
	Summer	54.93	46.51	44.94	46.20	47.29	43.24	38.30
	Annual	*385.55*	*354.93*	*363.58*	*364.15*	*362.78*	*353.93*	*318.18*
Spillway release (hm^3/year)	Autumn	6.69	9.68	10.16	11.53	11.18	10.93	11.33
	Winter	5.34	8.09	12.66	13.96	9.22	15.02	22.08
	Spring	104.70	69.12	65.44	63.05	68.35	51.62	32.27
	Summer	0.05	0.00	0.04	0.25	0.03	0.37	0.00
	Annual	*116.79*	*86.90*	*88.29*	*88.79*	*88.79*	*77.95*	*65.68*
Spillway release (day/year)	Autumn	2	2	2	2	2	2	2
	Winter	2	3	3	5	2	5	6
	Spring	32	22	20	19	22	16	8
	Summer	0	0	0	0	0	0	0
	Annual	*36*	*27*	*25*	*26*	*26*	*23*	*16*
Non-power release (hm^3/year)	Autumn	4.26	3.66	3.53	3.53	3.62	3.49	3.18
	Winter	12.59	12.58	12.58	12.58	12.58	12.58	12.58
	Spring	45.45	45.50	45.59	45.62	45.55	45.63	45.22
	Summer	6.12	6.12	6.12	6.12	6.12	6.12	6.12
	Annual	*68.42*	*67.86*	*67.82*	*67.85*	*67.87*	*67.82*	*67.10*
Environmental water deficiency (%)	Autumn	22.5	33.5	35.8	35.8	34.1	36.5	42.2
	Winter	0.0	0.0	0.0	0.0	0.0	0.0	0.0
	Spring	0.7	0.6	0.4	0.3	0.5	0.3	1.2
	Summer	0.0	0.0	0.0	0.0	0.0	0.0	0.0
	Annual	*2.2*	*3.0*	*3.1*	*3.0*	*3.0*	*3.1*	*4.1*

5. CONCLUSIONS

This assessment explores how climate change alters the hydropower production of a run-of-river type plant located in the most vulnerable highlands region of the ETRB, focusing on the Basoren Weir and HPP Project. Future energy projections of this assessment rely on the inflow time series derived from the SWAT runs. These runs are performed with the bias-adjusted precipitation and

temperature simulations from the 24 GCMs under the reference HEXP scenario and the moderate- and high-end future development scenarios of SSP2-4.5 and SSP5-8.5. By evaluating the energy production capacity from 1988 to 2009 as the benchmark scenario, the study seeks to determine whether the Basoren Project, designed using historical runoff records, can meet the expected hydropower production in the periods of 2025-2049, 2050-2074, and 2075-2099. To address the uncertainty stemming from varying projections of GCMs and, hence, inflow time series, this study adopts a strategy wherein the median values of the operational results for the climate projections from each GCM are considered in quantifying the potential future changes in the energy production capacity of the Basoren HPP. The results reveal potential decreases of 7.9%, 5.5%, and 5.3% under the SSP2-4.5 scenario, and 5.8%, 8.0%, and 17.3% under the SSP5-8.5 scenario in the mean annual energy output of the Basoren HPP for the periods of 2025-2049, 2050-2074, and 2075-2099, respectively. Although the projected decreases in the amount of spillway release are expected to partially mitigate the impacts of decreasing streamflow rates on energy production over these three future periods, it is clear that the anticipated shift in the hydrologic regime from snow-dominated to rain-dominated, as noted in other studies [47,48], necessitates re-optimizing the installed power capacities of the plants in the ETRB to sustain the appropriate use of the basin's hydropower potential. For future studies aimed at designing plant units under changing climate impacts, it is highly recommended to utilize climate projections derived from CMIP6-based RCMs, which are poised to become widely accessible in the forthcoming years, to provide more detailed and region-specific projections of climate variables, enabling more accurate and effective adaptation and mitigation strategies.

DECLARATION OF ETHICAL STANDARDS

The author of the paper submitted declares that nothing which is necessary for achieving the paper requires ethical committee and/or legal-special permissions.

CONTRIBUTION OF THE AUTHORS

Emrah Yalcin: Conceptualization, methodology, writing - review and editing.

CONFLICT OF INTEREST

There is no conflict of interest in this study.

REFERENCES

[1] Haddeland I, Heinke J, Biemans H, Eisner S, Flörke M, Hanasaki N, Konzmann M, Ludwig F, Masaki Y, Schewe J, Stacke T, Tessler ZD, Wada Y, Wisser D. Global water resources affected by human interventions and climate change. Proceedings of the National Academy of Sciences 2014; 111(9): 3251-3256.

[2] IPCC (Intergovernmental Panel on Climate Change). Climate change 2021: The physical science basis, contribution of working group I to the IPCC sixth assessment report. In: Masson-Delmotte V, Zhai P, Pirani A, Connors SL, Péan C, Berger S, Caud N, Chen Y, Goldfarb L, Gomis MI, Huang M, Leitzell K, Lonnoy E, Matthews JBR, Maycock TK, Waterfield T, Yelekçi O, Yu R, Zhou B (eds). Cambridge University Press, Cambridge and New York, 2021.

[3] Konapala G, Mishra AK, Wada Y, Mann ME. Climate change will affect global water availability through compounding changes in seasonal precipitation and evaporation. Nature Communications 2020; 11: 3044.

[4] Piao S, Ciais P, Huang Y, Shen Z, Peng S, Li J, Zhou L, Liu H, Ma Y, Ding Y, Friedlingstein P, Liu C, Tan K, Yu Y, Zhang T, Fang J. The impacts of climate change on water resources and agriculture in China. Nature 2010; 467: 43-51.

[5] Pokhrel Y, Felfelani F, Satoh Y, Boulange J, Burek P, Gädeke A, Gerten D, Gosling SN, Grillakis M, Gudmundsson L, Hanasaki N, Kim H, Koutroulis A, Liu J, Papadimitriou L, Schewe J, Schmied HM, Stacke T, Telteu C-E, Thiery W, Veldkamp T, Zhao F, Wada Y. Global terrestrial water storage and drought severity under climate change. Nature Climate Change 2021; 11: 226-233.

[6] Dolan F, Lamontagne J, Link R, Hejazi M, Reed P, Edmonds J. Evaluating the economic impact of water scarcity in a changing world. Nature Communications 2021; 12: 1915.

[7] Monier E, Paltsev S, Sokolov A, Chen Y-HH, Gao X, Ejaz Q, Couzo E, Schlosser CA, Dutkiewicz S, Fant C, Scott J, Kicklighter D, Morris J, Jacoby H, Prinn R, Haigh M. Toward a consistent modeling framework to assess multi-sectoral climate impacts. Nature Communications 2018; 9: 660.

[8] Almeida RM, Fleischmann AS, Brêda JPF, Cardoso DS, Angarita H, Collischonn W, Forsberg B, García-Villacorta R, Hamilton SK, Hannam PM, Paiva R, Poff NL, Sethi SA, Shi Q, Gomes CP, Flecker AS. Climate change may impair electricity generation and economic viability of future Amazon hydropower. Global Environmental Change 2021; 71: 102383.

[9] Ceribasi G, Caliskan M. Short- and long-term prediction of energy to be produced in hydroelectric energy plants of Sakarya Basin in Turkey. Energy Sources, Part A: Recovery,

Utilization, and Environmental Effects 2023; 45(1): 2680-2695.
[10] Ceribasi G, Ceyhunlu AI, Wałęga A, Młyński D. Investigation of the effect of climate change on energy produced by hydroelectric power plants (HEPPs) by trend analysis method: A case study for Dogancay I–II HEPPs. Energies 2022; 15(7): 2474.
[11] Gernaat DEHJ, de Boer HS, Daioglou V, Yalew SG, Müller C, van Vuuren DP. Climate change impacts on renewable energy supply. Nature Climate Change 2021; 11: 119-125.
[12] IHA (International Hydropower Association). Hydropower status report 2018. International Hydropower Association, Paris, 2018.
[13] Pereira-Cardenal SJ. Water-energy modelling: Adaptation to water scarcity. Nature Energy 2016; 1: 16004.
[14] Pir H, Ceribasi G, Ceyhunlu AI. The effect of climate change on energy generated at hydroelectric power plants: A case of Sakarya river basin in Turkey. Renewable Energy 2024; 223: 120077.
[15] van Vliet MTH, Wiberg D, Leduc S, Riahi K. Power-generation system vulnerability and adaptation to changes in climate and water resources. Nature Climate Change 2016; 6: 375-380.
[16] Yalew SG, van Vliet MTH, Gernaat DEHJ, Ludwig F, Miara A, Park C, Byers E, Cian ED, Piontek F, Iyer G, Mouratiadou I, Glynn J, Hejazi M, Dessens O, Rochedo P, Pietzcker R, Schaeffer R, Fujimori S, Dasgupta S, Mima S, da Silva SRS, Chaturvedi V, Vautard R, van Vuuren DP. Impacts of climate change on energy systems in global and regional scenarios. Nature Energy 2020; 5: 794-802.
[17] Zhou Q, Hanasaki N, Fujimori S, Masaki Y, Hijioka Y. Economic consequences of global climate change and mitigation on future hydropower generation. Climatic Change 2018; 147: 77-90.
[18] Carvajal PE, Anandarajah G, Mulugetta Y, Dessens O. Assessing uncertainty of climate change impacts on long-term hydropower generation using the CMIP5 ensemble - The case of Ecuador. Climatic Change 2017; 144: 611-624.
[19] Lumbroso DM, Woolhouse G, Jones L. A review of the consideration of climate change in the planning of hydropower schemes in sub-Saharan Africa. Climatic Change 2015; 133: 621-633.
[20] Mukheibir P. Potential consequences of projected climate change impacts on hydroelectricity generation. Climatic Change 2013; 121: 67-78.
[21] Natalia P, Silvia F, Silvina S, Miguel P. Climate change in northern Patagonia: Critical decrease in water resources. Theoretical and Applied Climatology 2020; 140: 807-822.
[22] Sharma N, Mishra BK, Baral S. Climate change impacts on Seti Gandaki River flow from

hydropower perspectives, Nepal. Sustainable Water Resources Management 2024; 10: 28.
[23] Liu X, Tang Q, Voisin N, Cui H. Projected impacts of climate change on hydropower potential in China. Hydrology and Earth System Sciences 2016; 20(8): 3343-3359.
[24] Ali SA, Aadhar S, Shah HL, Mishra V. Projected increase in hydropower production in India under climate change. Scientific Reports 2018; 8: 12450.
[25] Hurford AP, Harou JJ, Bonzanigo L, Ray PA, Karki P, Bharati L, Chinnasamy P. Efficient and robust hydropower system design under uncertainty - A demonstration in Nepal. Renewable and Sustainable Energy Reviews 2020; 132: 109910.
[26] Meng Y, Liu J, Leduc S, Mesfun S, Kraxner F, Mao G, Qi W, Wang Z. Hydropower production benefits more from 1.5°C than 2°C climate scenario. Water Resources Research 2020; 55: e2019WR025519.
[27] O'Neill BC, Tebaldi C, van Vuuren DP, Eyring V, Friedlingstein P, Hurtt G, Knutti R, Kriegler E, Lamarque J-F, Lowe J, Meehl GA, Moss R, Riahi K, Sanderson BM. The Scenario Model Intercomparison Project (ScenarioMIP) for CMIP6. Geoscientific Model Development 2016; 9(9): 3461-3482.
[28] Riahi K, van Vuuren DP, Kriegler E, Edmonds J, Neill BCO, Fujimori S, Bauer N, Calvin K, Dellink R, Fricko O, Lutz W, Popp A, Cuaresma JC, Samir KC, Leimbach M, Jiang L, Kram T, Rao S, Emmerling J, Ebi K, Hasegawa T, Havlik P, Humpenöder F, Da Silva LA, Smith S, Stehfest E, Bosetti V, Eom J, Gernaat D, Masui T, Rogelj J, Strefler J, Drouet L, Krey V, Luderer G, Harmsen M, Takahashi K, Baumstark L, Doelman JC, Kainuma M, Klimont Z, Marangoni G, Lotze-Campen H, Obersteiner M, Tabeau A, Tavoni M. The Shared Socioeconomic Pathways and their energy, land use, and greenhouse gas emissions implications: An overview. Global Environmental Change 2017; 42: 153-168.
[29] Cook BI, Mankin JS, Marvel K, Williams AP, Smerdon JE, Anchukaitis KJ. Twenty-first century drought projections in the CMIP6 forcing scenarios. Earth's Future 2020; 8(6): e2019EF001461.
[30] Dosio A, Jury MW, Almazroui M, Ashfaq M, Diallo I, Engelbrecht FA, Klutse NAB, Lennard C, Pinto I, Sylla MB, Tamoffo AT. Projected future daily characteristics of African precipitation based on global (CMIP5, CMIP6) and regional (CORDEX, CORDEX-CORE) climate models. Climate Dynamics 2021; 57: 3135-3158.
[31] Turner AG, Annamalai H. Climate change and the South Asian summer monsoon. Nature Climate Change 2012; 2: 587-595.
[32] Lee D-K, Cha D-H. Regional climate modeling for Asia. Geoscience Letters 2020; 7: 13.

[33] Daggupati P, Srinivasan R, Ahmadi M, Verma D. Spatial and temporal patterns of precipitation and stream flow variations in Tigris-Euphrates river basin. Environmental Monitoring and Assessment 2017; 189(2): 50.

[34] Giorgi F. Climate change hot-spots. Geophysical Research Letters 2006; 33(8): L08707.

[35] Lelieveld J, Hadjinicolaou P, Kostopoulou E, Chenoweth J, El Maayar M, Giannakopoulos C, Hannides C, Lange MA, Tanarhte M, Tyrlis E, Xoplaki E. Climate change and impacts in the Eastern Mediterranean and the Middle East. Climatic Change 2012; 114(3-4): 667-687.

[36] Zittis G, Almazroui M, Alpert P, Ciais P, Cramer W, Dahdal Y, Fnais M, Francis D, Hadjinicolaou P, Howari F, Jrrar A, Kaskaoutis DG, Kulmala M, Lazoglou G, Mihalopoulos N, Lin X, Rudich Y, Sciare J, Stenchikov G, Xoplaki E, Lelieveld J. Climate change and weather extremes in the Eastern Mediterranean and Middle East. Reviews of Geophysics 2022; 60(3): e2021RG000762.

[37] Bozkurt D, Sen OL. Climate change impacts in the Euphrates-Tigris Basin based on different model and scenario simulations. Journal of Hydrology 2013; 480: 149-161.

[38] Bozkurt D, Sen OL, Hagemann S. Projected river discharge in the Euphrates-Tigris Basin from a hydrological discharge model forced with RCM and GCM outputs. Climate Research 2015; 62(2): 131-147.

[39] Sen OL, Unal A, Bozkurt D, Kindap T. Temporal changes in the Euphrates and Tigris discharges and teleconnections. Environmental Research Letters 2011; 6(2): 024012.

[40] Yucel I, Güventürk A, Sen OL. Climate change impacts on snowmelt runoff for mountainous transboundary basins in eastern Turkey. International Journal of Climatology 2015; 35(2): 215-228.

[41] Chenoweth J, Hadjinicolaou P, Bruggeman A, Lelieveld J, Levin Z, Lange MA, Xoplaki E, Hadjikakou M. Impact of climate change on the water resources of the eastern Mediterranean and Middle East region: Modeled 21st century changes and implications. Water Resources Research 2011; 47(6): W06506.

[42] Kitoh A, Yatagai A, Alpert P. First super-high-resolution model projection that the ancient "Fertile Crescent" will disappear in this century. Hydrological Research Letters 2008; 2: 1-4.

[43] Nohara D, Kitoh A, Hosaka M, Oki T. Impact of climate change on river discharge projected by multimodel ensemble. Journal of Hydrometeorology 2006; 7(5): 1076-1089.

[44] Özdoğan M. Climate change impacts on snow water availability in the Euphrates-Tigris basin. Hydrology and Earth System Sciences 2011; 15(9): 2789-2803.

[45] Şen Z. Climate change expectations in the upper Tigris River basin, Turkey. Theoretical and

Applied Climatology 2019; 137: 1569-1585.
[46] Şensoy A, Uysal G, Doğan YO, Civelek HS. The future snow potential and snowmelt runoff of Mesopotamian water tower. Sustainability 2023; 15(8): 6646.
[47] Yalcin E. Assessing future changes in flood frequencies under CMIP6 climate projections using SWAT modeling: A case study of Bitlis Creek, Turkey. Journal of Water and Climate Change 2024; jwc2024646.
[48] Yalcin E. Quantifying climate change impacts on hydropower production under CMIP6 multi-model ensemble projections using SWAT model. Hydrological Sciences Journal 2023; 68(13): 1915-1936.
[49] AE SU (AE SU Engineering Limited Company). Basoren Weir and HPP feasibility report. AE SU Engineering Limited Company, Ankara, 2009.
[50] DSI (General Directorate of State Hydraulic Works). Electrical Power Resources Survey and Development Administration (EIE) - Stream gauging yearbooks (1935-2011). General Directorate of State Hydraulic Works, Ankara, 2022.
[51] MGM (Turkish State Meteorological Service). Long-term all parameters bulletin for the Bitlis (Station ID: 17207) and Siirt (Station ID: 17210) weather stations. Turkish State Meteorological Service, Ankara, 2022.
[52] MGM (Turkish State Meteorological Service). Daily precipitation, maximum and minimum air temperature, wind speed, solar radiation, and relative humidity records of the Bitlis (Station ID: 17207) and Siirt (Station ID: 17210) weather stations. Turkish State Meteorological Service, Ankara, 2022.
[53] Arnold JG, Kiniry JR, Srinivasan R, Williams JR, Haney EB, Neitsch SL. SWAT 2012 input/output documentation. Texas Water Resources Institute, Texas, 2013.
[54] Neitsch SL, Arnold JG, Kiniry JR, Williams JR. Soil and Water Assessment Tool theoretical documentation version 2009. Texas Water Resources Institute, Texas, 2011.
[55] USGS (United States Geological Survey). Shuttle Radar Topography Mission (SRTM): 1 arc-second global elevation database. United States Geological Survey, 2014. https://earthexplorer.usgs.gov/ (Accessed 28 June 2022).
[56] EC-JRC (European Commission - Joint Research Centre). The Global Land Cover 2000 (GLC2000) products. European Commission - Joint Research Centre, 2006. https://forobs.jrc.ec.europa.eu/products/glc2000/products.php (Accessed 28 June 2022).
[57] FAO (Food and Agriculture Organization of the United Nations). Digital Soil Map of the World (DSMW). Food and Agriculture Organization of the United Nations, 2007.

https://www.fao.org/geonetwork/srv/en/metadata.show?id=14116 (Accessed 28 June 2022).
[58] Abbaspour KC. SWAT-CUP2: SWAT calibration and uncertainty programs - A user manual. Eawag - Swiss Federal Institute of Aquatic Science and Technology, Duebendorf, 2015.
[59] Abbaspour KC, Johnson CA, van Genuchten MT. Estimating uncertain flow and transport parameters using a sequential uncertainty fitting procedure. Vadose Zone Journal 2004; 3(4): 1340-1352.
[60] Abbaspour KC, Yang J, Maximov I, Siber R, Bogner K, Mieleitner J, Zobrist J, Srinivasan R. Modelling hydrology and water quality in the pre-alpine/alpine Thur watershed using SWAT. Journal of Hydrology 2007; 333(2-4): 413-430.
[61] Abbaspour KC, Rouholahnejad E, Vaghefi S, Srinivasan R, Yang H, Kløve B. A continental-scale hydrology and water quality model for Europe: Calibration and uncertainty of a high-resolution large-scale SWAT model. Journal of Hydrology 2015; 524: 733-752.
[62] Yalcin E. Estimation of irrigation return flow on monthly time resolution using SWAT model under limited data availability. Hydrological Sciences Journal 2019; 64(13): 1588-1604.
[63] Nash JE, Sutcliffe JV. River flow forecasting through conceptual models part I - A discussion of principles. Journal of Hydrology 1970; 10(3): 282-290.
[64] ESGF (Earth System Grid Federation). WCRP Coupled Model Intercomparison Project (Phase 6). Earth System Grid Federation, 2022. https://esgf-node.llnl.gov/projects/cmip6/ (Accessed 15 May 2022).
[65] Jones PW. First- and second-order conservative remapping schemes for grids in spherical coordinates. Monthly Weather Review 1999; 127(9): 2204-2210.
[66] Rathjens H, Bieger K, Srinivasan R, Chaubey I, Arnold JG. CMhyd user manual: Documentation for preparing simulated climate change data for hydrologic impact studies. Purdue University, United States Department of Agriculture - Agricultural Research Service, Texas A&M AgriLife, and Texas A&M University, 2016. https://swat.tamu.edu/media/115265/bias_cor_man.pdf (Accessed 25 May 2022).
[67] Legates DR, McCabe GJ. Evaluating the use of "goodness-of-fit" measures in hydrologic and hydroclimatic model validation. Water Resources Research 1999; 35(1): 233-241.
[68] Almeida MP, Perpiñán O, Narvarte L. PV power forecast using a nonparametric PV model. Solar Energy 2015; 115: 354-368.
[69] Gupta HV, Kling H, Yilmaz KK, Martinez GF. Decomposition of the mean squared error and NSE performance criteria: Implications for improving hydrological modelling. Journal of Hydrology 2009; 377(1-2): 80-91.

[70] Roberts NM, Lean HW. Scale-selective verification of rainfall accumulations from high-resolution forecasts of convective events. Monthly Weather Review 2008; 136(1): 78-97.
[71] Moriasi DN, Gitau MW, Pai N, Daggupati P. Hydrologic and water quality models: Performance measures and evaluation criteria. Transactions of the ASABE 2015; 58(6): 1763-1785.
[72] Moriasi DN, Arnold JG, Van Liew MW, Bingner RL, Harmel RD, Veith TL. Model evaluation guidelines for systematic quantification of accuracy in watershed simulations. Transactions of the ASABE 2007; 50(3): 885-900.
[73] Ahmed K, Sachindra DA, Shahid S, Demirel MC, Chung E-S. Selection of multi-model ensemble of general circulation models for the simulation of precipitation and maximum and minimum temperature based on spatial assessment metrics. Hydrology and Earth System Sciences 2019; 23(11): 4803-4824.
[74] Bağçaci SÇ, Yucel I, Duzenli E, Yilmaz MT. Intercomparison of the expected change in the temperature and the precipitation retrieved from CMIP6 and CMIP5 climate projections: A Mediterranean hot spot case, Turkey. Atmospheric Research 2021; 256: 105576.
[75] Seker M, Gumus V. Projection of temperature and precipitation in the Mediterranean region through multi-model ensemble from CMIP6. Atmospheric Research 2022; 280: 106440.